Supplementary material

All-optical control of the quantum flow of a polariton condensate

D. Sanvitto[1], S. Pigeon[2], A. Amo[3,4], D. Ballarini[5], M. De Giorgi[1], I. Carusotto[6], R. Hivet[3], F. Pisanello[3], V. G. Sala[3], P. S. S. Guimaraes[7], R. Houdré[8], E. Giacobino[3], C. Ciuti[2], A. Bramati[3], G. Gigli[1,5]

[1] NNL, Istituto Nanoscienze - CNR, Via Arnesano, 73100 Lecce, Italy
[2] Laboratoire Matériaux et Phénomènes Quantiques, UMR 7162, Université Paris Diderot-Paris 7 et CNRS, 75013 Paris, France
[3] Laboratoire Kastler Brossel, Université Pierre et Marie Curie-Paris 6, École Normale Supérieure et CNRS, UPMC Case 74, 4 place Jussieu, 75005 Paris, France
[4] CNRS-Laboratoire de Photonique et Nanostructures, Route de Nozay, 91460 Marcoussis, France
[5] Istituto Italiano di Tecnologia, IIT-Lecce, Via Barsanti, 73010 Lecce, Italy
[6] INO-CNR BEC Center and Dipartimento di Fisica, Università di Trento, I-38123 Povo, Italy
[7] Departamento de Física, Universidade Federal de Minas Gerais, Belo Horizonte MG, Brazil
[8] Institut de Physique de la Matière Condensée, Faculté des Sciences de Base, bâtiment de Physique, Station 3, EPFL, CH-1015 Lausanne, Switzerland

Sample description

The sample consists of a planar heterostructure containing three $In_{0.04}Ga_{0.96}As$ quantum wells with a thickness of 80 Å placed at the antinode of a planar microcavity. The Distributed Bragg Refrector (DBR) mirrors embedding the cavity are formed by 21 and 24 AlGaAs/AlAs alternated pairs in the top and bottom of the microcavity. At a temperature of 10 K, a Rabi splitting of 5.1 meV has been measured with polariton linewidths of the order of 0.1 meV. The wedge-shaped cavity allows for fine-tuning of the resonance between the quantum well exciton and the cavity mode by changing the position of the excitation spot on the sample.

Experimental details

Time resolved real space images of the polariton field are obtained in transmission geometry with the use of a synchroscan streak camera. A 80 fs pulsed Ti:sapphire laser is split into two beams: one is used to generate the polariton fluid whereas the second beam, stretched in time up to about a hundred of picoseconds, is used as reference to realize the interferograms from which the real-space phase pattern is inferred. During the time of the experiment any energy variation between the reference coming from the laser and the polariton condensate could cause a phase shift in the interference fringes. However, given the short time of the experiment (~40 ps) and the fact that the blue shift is mainly caused by the exciton reservoir (almost absent in our experimental geometry), this effect is negligible in the interference images.

Half of the excitation laser spot is completely masked by a metallic mask in order to avoid any influence of the driving field in the phase of the polariton condensate. The coherent emission collected by an aspheric lens with NA=0.61 is passed through a delay line in order to obtain the interference between the cavity emission and the reference beam and it is focused onto the slits of a monocromator coupled to a streak camera with a time resolution of 2 ps. An integration time of 1s for each snapshot has been used to acquire the data.

It is important to remind that the time resolved data are the result of the integration of several billions of nominally identical single realizations: the fact that vortices are visible in the averaged images proves that, in contrast to the purely CW experiment, they are formed at the same position and follow the same trajectory at each shot.

In the second part of the trapping vortices experiment, a CW ring laser with an in plane k≠0 is sent against a natural defect present in the microcavity. A hollow barrier potential is created behind the defect in different position relative to the Gaussian spot by using a triangular metallic mask. In this case the interferograms are obtained by the interference between the emission of the polariton state and a part of that expanded 4 times, in order to give a constant phase around the polariton area. Vortices are visible (both as a darker spot in the real images and as a fork-like dislocation in the interferences) whenever the triangular mask is set behind the natural defect. As soon as the mask is shifted away from the ~ 60° cone generated by the flow with a velocity of 0.9 μm/ps (k=0.38 μm^{-1}) against the defect (as is the case of ~ 50 μm downwards in Fig. 4e and 4k) no vortex is present in the triangular dark region. It is important to note that this regime is very different from the previous one, since here the pumping laser is a continuous wave and so only the steady state is observable in the images (no transient time for switching on or off is detectable). For this reason the visible vortices are the ones which stays in the same position for macroscopic times. Any fluctuation or movement from the defect to the trapping point is smeared out in time and could result in regions of reduced fringe contrast (as observable in some points of Fig. 4j and 4l).

For the realization of the quantum flow dynamics we have monitored the k-dependence of the polariton emission at given points of their trajectories, as shown in Fig. 1S. We have collected the far field emission out of a confocal system to be able to spatially select the contribution from three regions along the polariton flow, centered around the points marked as A, B and C in Fig. 1Sa. In all cases we see only one state occupied which demonstrate that no other interaction with the polaritons created in the CW spot is taking place (Fig. 1Sb). As expected for a flow diverted by the optical defect, the original k-vector (point A) is accelerated in the y-direction (points B and C) as shown in Fig. 1Sd. Conversely, along the x-direction, we can notice that the k-vector acquires a positive value in point C and a negative value in point B, consistent with a polariton flowing around the obstacle (Fig. 1Sc).

Calculation of the sound speed and polariton density

A rough estimation of the sound speed can be obtained from the aperture angle α of the Čerenkov-like conical density modulation [1] that is visible past the defect in the time-integrated images via the relation $\sin(\alpha/2)=c_s/v_f$ [2].

A quantitative estimation of the polariton density $|\psi|^2$ at the vortex nucleation points can be done by using the equation $c_s = \sqrt{\hbar g |\psi|^2/m}$, where g is the polariton-polariton interaction constant, m is the

effective mass of the lower polariton branch ($\sim 6 \times 10^{-5}$ m_0, with m_0 the free electron mass) and c_s is the sound speed.

The value of c_s at the point where the flow first meets the defect can be estimated from the Cerenkov angle as explained above. For different values of the CW power equal to 6 mW (Fig. 3a), 26 mW (Fig. 3b) and 52 mW (Fig. 3c), the estimated speed of sound is 0.3 µm/ps, 0.4 µm/ps and 0.5 µm/ps, respectively. The corresponding increase of the polariton density goes from $|\psi|^2$ = 9.5 µm^{-2} , to $|\psi|^2$ =12.4 µm^{-2} and $|\psi|^2$ = 15.9 µm^{-2}, respectively. This calculation is confirmed by the direct estimation of the density from the experimentally measured intensity of the emitted polaritons (8 µm^{-2}, 11 µm^{-2}, 14 µm^{-2}, respectively), which demonstrates the direct relation between the changes in c_s and the ones in the local density variation due to polariton decay. Moreover this effect is also responsible for the shift of the vortex nucleation point towards the equator (being defined as perpendicular to the direction of the polariton flow).

A comparison between the experimental and theoretical trajectories shown in Fig. 3a-c is plotted in figure 2S.

Theoretical details

To simulate the data presented in Fig. 2 and Fig. 1S we have used a spin-dependent Gross-Pitaevskii equation with pumping and decay which takes into account for the dynamics of the injected polariton population at a given time as well as the CW steady state population which is used to generate the defect. The equation can be written in the following way:

$$i\frac{d}{dt}\begin{pmatrix}\psi_{C\uparrow}(\mathbf{x},t)\\ \psi_{C\downarrow}(\mathbf{x},t)\\ \psi_{X\uparrow}(\mathbf{x},t)\\ \psi_{X\downarrow}(\mathbf{x},t)\end{pmatrix} = \begin{pmatrix}F_{p\uparrow}\\ F_{p\downarrow}\\ 0\\ 0\end{pmatrix}f_p(\mathbf{x},t)e^{i(\mathbf{k}_p\mathbf{x}-\omega_p t)} + \begin{pmatrix}F_{c\uparrow}\\ F_{c\downarrow}\\ 0\\ 0\end{pmatrix}e^{i(\mathbf{k}_c\mathbf{x}-\omega_c t)}e^{\frac{(\mathbf{x}-\mathbf{x}_{c0})^2}{2\delta_c^2}} + \mathbf{h^1}\begin{pmatrix}\psi_{C\uparrow}(\mathbf{x},t)\\ \psi_{C\downarrow}(\mathbf{x},t)\\ \psi_{X\uparrow}(\mathbf{x},t)\\ \psi_{X\downarrow}(\mathbf{x},t)\end{pmatrix}$$

where,

$$\mathbf{h^1} = \mathbf{h^0} + \begin{pmatrix}-i\frac{\gamma_C}{2} & 0 & 0 & 0\\ 0 & -i\frac{\gamma_C}{2} & 0 & 0\\ 0 & 0 & g_{\uparrow\uparrow}|\psi_{X\uparrow}|^2 + g_{\uparrow\downarrow}|\psi_{X\downarrow}|^2 - i\frac{\gamma_X}{2} & 0\\ 0 & 0 & 0 & g_{\downarrow\downarrow}|\psi_{X\downarrow}|^2 + g_{\downarrow\uparrow}|\psi_{X\uparrow}|^2 - i\frac{\gamma_X}{2}\end{pmatrix}$$

and

$$\mathbf{h^0} = \begin{pmatrix} \omega_C(-i\nabla) & 0 & \Omega_R & 0 \\ 0 & \omega_C(-i\nabla) & 0 & \Omega_R \\ \Omega_R & 0 & \omega_X & 0 \\ 0 & \Omega_R & 0 & \omega_X \end{pmatrix}.$$

- $F_{p\sigma}$ and $F_{c\sigma}$ are the amplitudes of the circularly polarized components ($\sigma+ =\uparrow$; $\sigma- =\downarrow$) of the pulsed and CW beams excitation fields, respectively, with. In our conditions of cross-linearly polarized pulsed and CW beams: $(F_{p\uparrow}, F_{p\downarrow}) = (F_p/\sqrt{2}, F_p/\sqrt{2})$ and $(F_{c\uparrow}, F_{c\downarrow}) = (F_c/\sqrt{2}, -iF_c/\sqrt{2})$
- $\psi_{C\uparrow(\downarrow)}(x,t)$ and $\psi_{X\uparrow(\downarrow)}(x,t)$ are, respectively, the photon and exciton complex fields with polarization $\sigma+$ ($\sigma-$).
- **x** is the position vector in the plane perpendicular to the growth direction (cavity plane; **x** = (x, y)).
- $\boldsymbol{k}_p$ ($\boldsymbol{k}_c$) is the wavevector of the pulsed (CW) beams.
- $f_p(\boldsymbol{x},t)$ is the spatial and temporal profile of the pulsed beam with a Fourier limited duration of 2 ps.
- The cw beam has a Gaussian shape centred at $\boldsymbol{x}_{c0}$ and width δ_0.
- $\hbar\gamma_C$ and $\hbar\gamma_X$ are the spectral widths of the cavity photons and excitons: 0.075 meV and 0.12 meV, respectively.
- $\hbar\omega_c$ is the energy of cw laser and $\hbar\omega_p$ is the central energy of the pulsed beam.
- $\hbar\Omega_R$ is the vacuum Rabi frequency (2.55meV), giving rise to a Rabi splitting of $2\hbar\Omega_R = 5.1\ meV$
- g_{ij} is the (exciton of polarization *i*)-(exciton of polarization *j*) interaction strength. The values used in the simulations are $g_{\uparrow\uparrow} = g_{\downarrow\downarrow} = 10g_{\downarrow\uparrow} = 10g_{\uparrow\downarrow}$, with $g_{\uparrow\uparrow} = 0.01$ meVμm^2.

References

[1] Amo, A. *et al.* Superfluidity of Polaritons in Semiconductor Microcavities. *Nature Phys.* **5**, 805-810 (2009).

[2] Carusotto, I., Hu, S. X., Collins, L. A. & Smerzi, A. Bogoliubov-Cerenkov Radiation in a Bose-Einstein Condensate Flowing against an Obstacle. *Phys. Rev. Lett.* **97**, 260403 (2006).

Supplementary video

The supplementary video "Video_Fig3e" shows the time resolved interferogram of the vortex and antivortex trajectory with the experimental parameters of Fig. 3e. Note the formation and annihilation of the topological defect generated by a shallow and small optical defect. The polariton condensate flows from left to right.
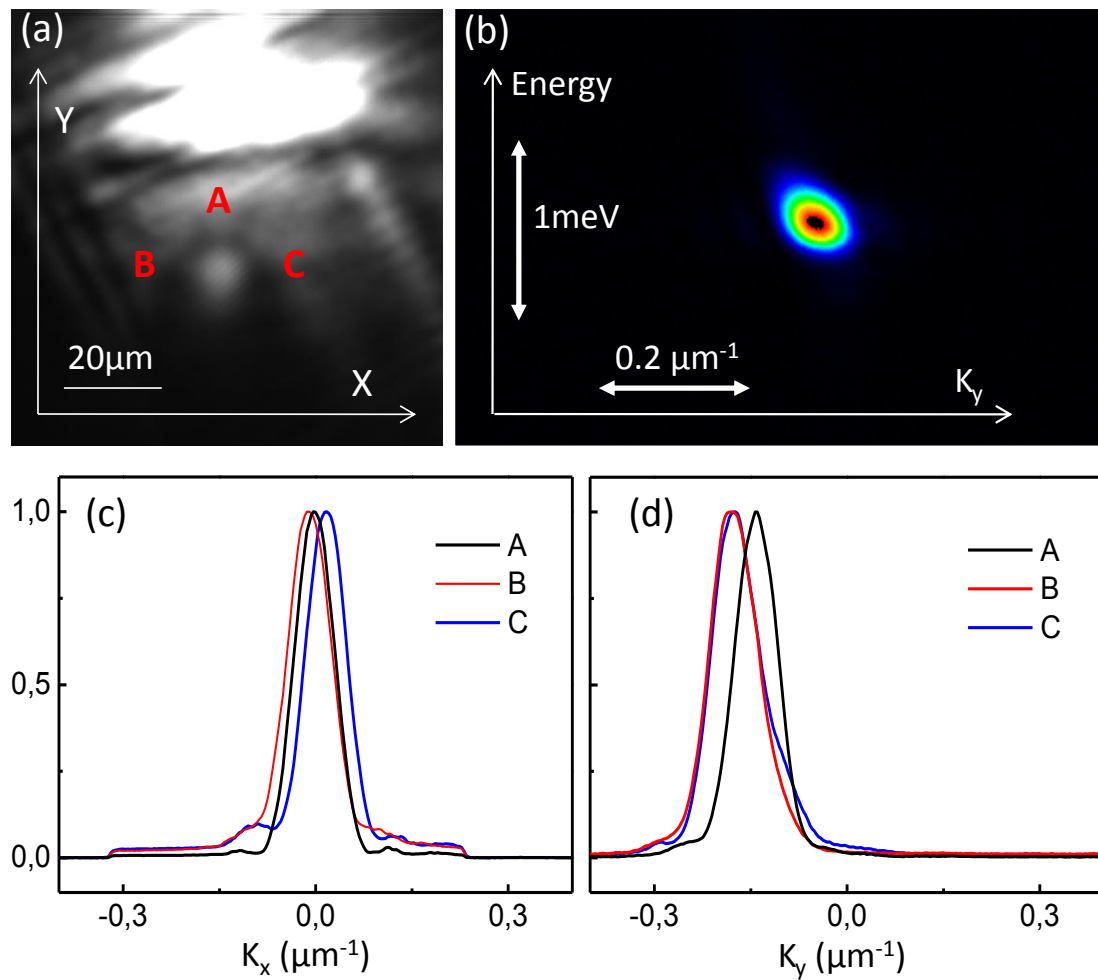
Supplementary figures

Fig. 1S: Panel (a) shows the time-integrated real-space emission of polaritons diverted by the optical defect. The flow is initially injected along the -y direction (from top to bottom). Panels (c) and (d): spatially-selected far field emission pattern from spatial regions around the points marked as A,B,C in panel (a). Panel (b) shows the energy-momentum dispersion of the spatially-selected emission from point A.
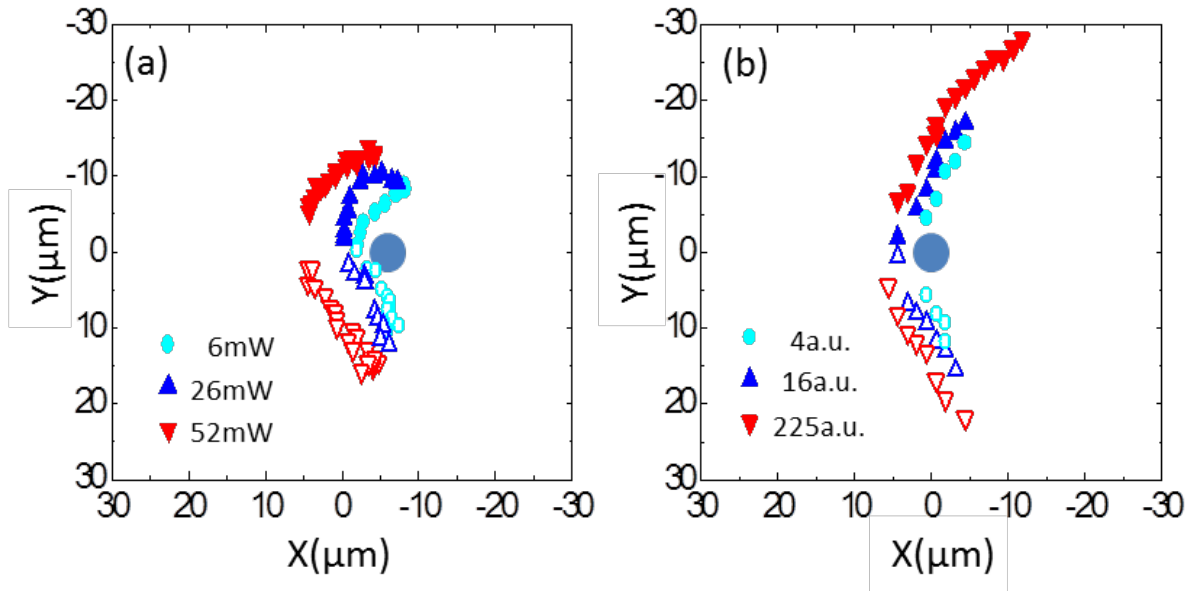
Fig. 2S: Panel (a) shows vortex/antivortex trajectories corresponding to the images of Fig. 3(a), (b) and (c). The trajectories are obtained for each temporal frame by recording the position of the center of the vortex core evidenced via the fork dislocation of the interference pattern (see Fig. 2). Panel (b) displays the theoretical trajectories of different simulation runs using increasing CW pump powers, showing the same trend observed in the experiments. The position of the defect potential is indicated by the blue circle.